Numerical Simulation and PIV Measurement on the Internal Flow in a Centrifugal Mini Pump at Low Flow Rate Conditions

Hui-jing Yuan YuanHJ@pku.edu.cn
Jie Shao shaojie00@mails.tsinghua.edu.cn
Guang-Jun Cao Guangjun_cao@163.com
Shu-Hong Liu liushuhong@mail.thu.edu.cn
Yu-lin Wu Wyl-dhh@mail.tsinghua.edu.cn

State Key Laboratory of Hydro-science and Engineering
Dept. of Thermal Engineering, Tsinghua University, Beijing 100084, China

Keywords: Mini Pump, PIV, LIF, Standard k-ε model, Low Flow Rate

ABSTRACT

This paper reports on the internal flow of a centrifugal mini pump working at the low flow rate operating conditions. The RNG k-ε turbulence model was employed to simulate the three-dimensional turbulent flow in the pump. To examine and certify the simulation results, a transparent acrylic centrifugal mini pump model which is suitable for PIV measurement has been developed. The tongue region and the passages region between blades were investigated using PIV. In order to eliminate the effect of refraction on the area closed to the wall and increase the measurement accuracy, the fluorescent particles were scatted into the working fluid with the tracing particles. It is found from the calculation and PIV measurement results that there is a large area of recirculation flow near the tongue at low flow rate operating conditions. The computationally predicted water head using the k-ε turbulence model at low flow rate operating conditions are in very good agreement with the experimentally measured water head and the mean velocity distributions at investigation area obtained by PIV and calculation showed a satisfactory agreement as well. Meanwhile, the results of PIV measurements show that the flow status in one passage is different to another. And for capturing the internal flow detail information, the k-ε turbulence model is not very suitable.

INTRODUCTION

Nowadays, the pumps of different size are needed by a great variety of calling. According to the specific dimension, the pumps can be divided into three categories, normal pump, mini pump and micro pump. The specific dimension of mini pump is from 1 mm to 50 mm. The mini pump is widely used in many fields, such as the aerospace vehicle, medical apparatus and instruments, fuel cell and so on.

In the past, both computational fluid dynamics (CFD) [1-2] and experimental flow visualization have been performed to reveal flow characteristics within mini pumps and peripherals to examine a specific design and guide design improvement. Li et al. [3] studied the interior viscous flow in a mini pump with an asymmetric axis using the PIV method. Nicholas Pedersen et al.[4] investigated the flow inside the rotating passages of a six-bladed shrouded centrifugal pump impeller using PIV and LDV. Jaikrishnan R. Kadambi et al.[5] utilized PIV to investigate the velocities and kinetic energy fluctuations of slurry particles at the tongue region of an optically-clear centrifugal pump. Most of the investigations are performed at design conditions, there is little research on the internal flow investigation at low flow rate operating conditions. Because the internal flow is complicated at low flow rate working conditions, and sometimes the mini pump should be used in that situation. The study on the internal flow of a mini pump at low flow rate working condition is necessary.

The specific dimension of the mini pump we designed is 37 mm. But to make the processing easier and satisfy the PIV measurement demand, the specific dimension of experimental pump model is enlarged to 100mm. In this paper the numerical simulation and PIV measurement of the pump have been carried out at low flow rate operating conditions.

EXPERIMENTAL APPARATUS

1. Centrifugal Impeller.

The impeller under investigation is a model centrifugal pump impeller that is used in a centrifugal mini pump. Figure 1 shows the geometry of the impeller. It consists of six two-dimensioned curvature backward swept blades of constant thickness and arc profile leading edges and blunt trailing edges. The axial height of the impeller blade is tapered linearly from 15.13 mm at the inlet to 8.11 mm at the outlet. The entire impeller is manufactured in acryl for the PIV measurements at impeller passages. Table 1 summarizes the main dimensions of the test impeller.

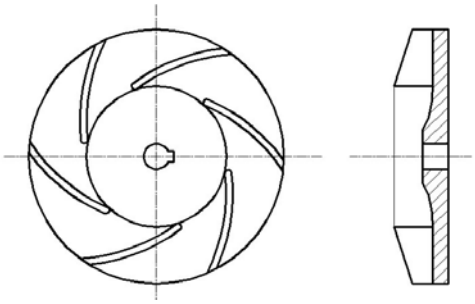

Fig. 1 Blade-to-blade and meridional view of the centrifugal impeller

Table 1 Impeller geometry

Geometry	Symbol	Value	Unit
Inlet diameter	D_1	55.14	mm
Outlet diameter	D_2	100	mm
Inlet height	b_1	15.13	mm
Outlet height	b_2	8.11	mm
Number of blades	Z	6	—
Blade thickness	t	2.7	mm
Inlet blade angle	β_1	15	deg.
Outlet blade angle	β_2	39	deg.

2. The Experimental Set-Up.

Mini-pump Loop Facility

An outline of the pump closed-loop is shown in Fig.2. The water flow rate is measured by an electromagnetic flowmeter which is located downstream of the pump discharge and controlled by the inlet and out regulating valves. The angular speed is controlled by an inverter and fixed to 1000rpm for this study. The water head is measured by two pressure sensors.

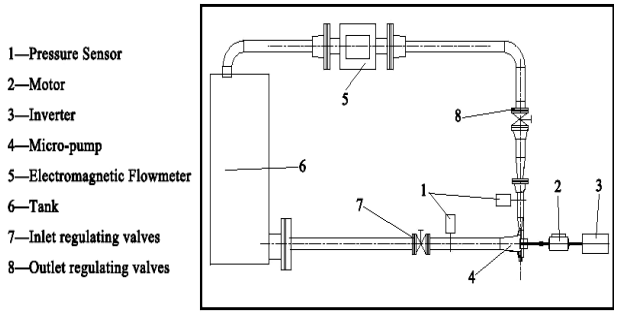

Fig. 2 The outline of the pump closed-loop

The flow in the loop is delivered by an optically clear centrifugal pump. The pump has a transparent casing and a transparent six-blade impeller. Control of the timing of the PIV laser firing as a function of impeller blade position is provided by a combination of an optical encoder placed 5cm away from the shaft of the centrifugal pump and a reflective surface marker on the shaft and aligned with one of the blades of the impeller.

The Optically Clear Centrifugal mini-pump

The pump is specially designed to provide optical access. The casing and the impeller of the pump (Fig.3) are made from optically transparent acrylic. The ratio of pump casing inlet diameter to the discharge diameter is 1.50. The impeller has six blades.

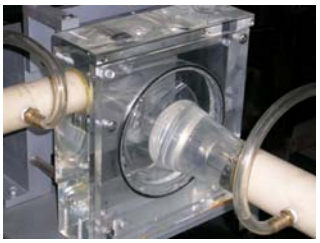

Fig. 3 Centrifugal pump with clear casing and clear impeller

PIV System

PIV is a technique that measures the instantaneous velocity field within an illuminated plane of the fluid field using light scattered from particles seeded into the fluid[6]. PIV has recently matured to a reliable technique that is used in a wide variety of applications[7]. Figure 4 shows the PIV setup. The PIV hardware consists of a 120mJ/pulse dual-cavity pulsed Nd:YAG laser, laser light sheet optics, a charge coupled device(CCD) camera, a synchronizer and a dates process system. We use the hollow spherical glass beads of 10 to 20 μm size as the tracing particles.

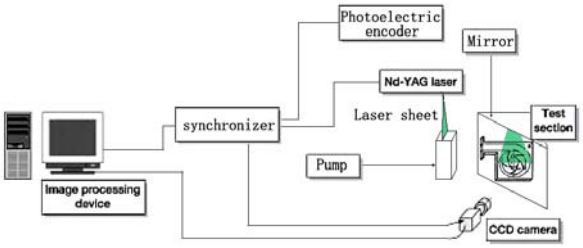

Fig. 4 PIV System setup

Figure 5 shows the regions of interest in the casing and impeller of the centrifugal mini pump. Because there is no room for the CCD to put after the pump to take pictures of the two regions, we put a mirror there, instead. So, the measurements could be performed through the mirror in the facility specially designed to provide an unobstructed view of the flow.

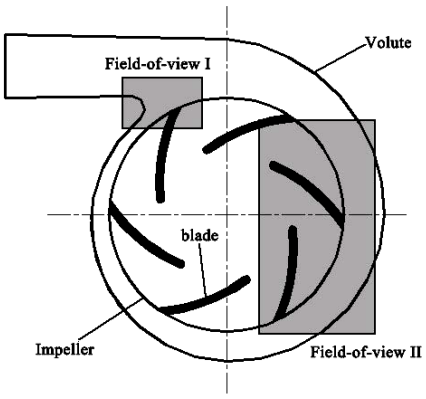

Fig. 5 Locations of the field of view in the centrifugal pump

A pair of single exposure image frames is required to enable cross-correlation date processing. The image pairs are processed into vector maps by the TSI Insight software. The image pair acquisition was synchronized to the impeller rotation using a synchronizer which located at the pump shaft. Besides, in order to investigate the flow details near the wall, the fluorescent particles were scatted into the fluid.

NUMERICAL SIMULATION

To compare with the experimental results, the numerical simulation has been carried out. The three-dimensional geometry model of the mini pump was generated using a 3-D modeling software package (Gambit, v2.2.60, Fluent Inc., Lebanon, NH, USA). The computational domains include the inlet, outlet, impeller and the volute. Then the geometry meshed by using the 3-D Tet/Hybid elements. The final meshes containing 0.88M Tetrahedral cells.

An unstructured-mesh finite-volume-based commercial CFD package, Fluent (v6.2.16,Fluent Inc.), was used to solve the incompressible steady Naiver-Stokes equations.

The incompressible continuity equation and Reynolds time averaged N-S equation are employed to simulate the flow through the pump, and k-ε double equations turbulent flow model is adopted to make the equations closed. The control equations are as follows:

The continuity equation is

$$\frac{\partial(\rho u_{\mathrm{i}})}{\partial x_{\mathrm{i}}} = 0 \qquad (1)$$

The momentum equation is

$$\frac{\partial(\rho u_{\mathrm{j}} u_{\mathrm{i}})}{\partial x_{\mathrm{j}}} = -\frac{\partial p^{*}}{\partial x_{\mathrm{i}}} + \frac{\partial\left[\mu_{eff}\left(\frac{\partial u_{\mathrm{i}}}{\partial x_{\mathrm{j}}} + \frac{\partial u_{\mathrm{j}}}{\partial x_{\mathrm{i}}}\right)\right]}{\partial x_{\mathrm{j}}} - 2\varepsilon_{\mathrm{ijk}} k\omega_{\mathrm{j}} u_{\mathrm{k}} \qquad (2)$$

Here μ_{eff} is the effective viscosity coefficient, which is

$$\mu_{eff} = \mu + \mu_{\mathrm{t}}$$

In standard k- ε model μ_t is the eddy viscosity, which is

$$\mu_{\mathrm{t}} = \rho c_{\mu} \frac{k^2}{\varepsilon}$$

The transport equations of the k and ε are

$$\frac{\partial}{\partial x_{\mathrm{j}}}[\rho u_{\mathrm{j}} k - (\mu + \frac{\mu_{\mathrm{t}}}{\sigma_{\mathrm{k}}})\frac{\partial k}{\partial x_{\mathrm{j}}}] = \rho(p_{\mathrm{k}} - \varepsilon)$$

$$\frac{\partial}{\partial x_{\mathrm{j}}}[\rho u_{\mathrm{j}} \varepsilon - (\mu + \frac{\mu_{\mathrm{t}}}{\sigma_{\varepsilon}})\frac{\partial \varepsilon}{\partial x_{\mathrm{j}}}] = \rho\frac{\varepsilon}{k}(c_1 p_{\mathrm{k}} - c_2\varepsilon) \qquad (3)$$

Here p_k is the production of turbulent kinetic energy, which is

$$p_{\mathrm{k}} = \frac{\mu_{\mathrm{t}}}{\rho}(\frac{\partial u_{\mathrm{i}}}{\partial x_{\mathrm{j}}} + \frac{\partial u_{\mathrm{j}}}{\partial x_{\mathrm{i}}})\frac{\partial u_{\mathrm{i}}}{\partial x_{\mathrm{j}}}$$

In the above equations the experiential coefficients are as follows:

$C_{\mu} = 0.09$, $C_1 = 1.44$, $C_2 = 1.92$, $\sigma_k = 1.0$, $\sigma_{\varepsilon} = 1.3$

The finite volume method is applied to make the control equations discrete in space under the unstructured mesh (see figure 6). The second-order central difference is applied to the source item and diffusion item of the control equations, and the second-order upwind difference is applied to the convection item. SIMPLEC algorithm is applied to solve the discrete equations.

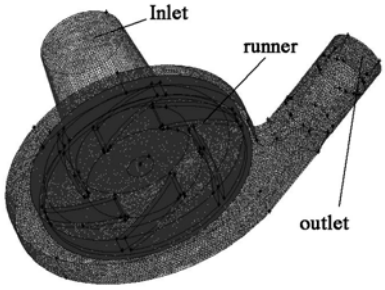

Fig. 6 The mesh of the whole passage

The boundary conditions are set as flows:

A mass-flow boundary condition was specified at the inlet and an outflow condition was set at the outlet. The wall function is adopted near the fixed wall, and non-slip boundary condition is adopted on the fixed wall. If the boundary is rotary, the angular speed of the boundary is set as ω_{r}.

RESULTS AND DISCUSSION

1. Hydrodynamic performance of the mini pump

The hydrodynamics pumping functions of the mini pump is shown in Fig.7. The pumping functions are expressed as the pump-generated water head versus

flow rate curve (H-Q curve) and the pump efficiency versus flow rate curve (η −Q curve) at the specific rotation speed (1000rpm). The CFD simulation was performed at 5 operating conditions (shown in Table 2). The flow rate of the operating conditions is only 8%~24% of the designed flow rate. The computationally predicted water head at these conditions are in very good agreement with the experimentally measured water head.

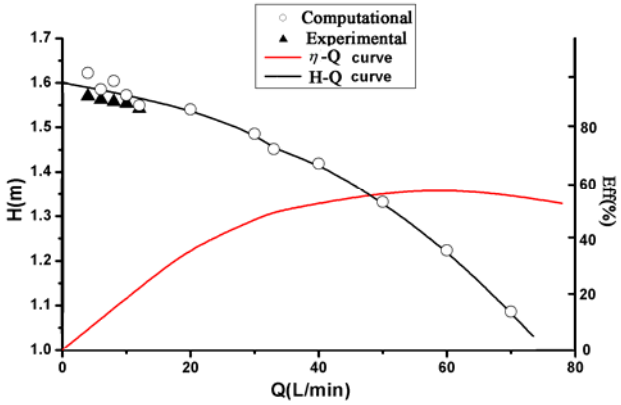

Fig. 7 The performance curve of mini pump

Table 2 Experimental operating conditions

Flow conditions	Symbol						Unit
Flow rate	Q	4	6	8	10	12	L/min
Rotational speed	n	1000					rpm
Test positions	—	Tongue		Impeller passage			—

2. The internal flow of the mini pump

The velocity magnitude distribution for the particles is obtained at two locations (see Fig. 5), which over tongue region (Field-of-view I) and the impeller passage (Field-of-view II). One hundred image frame pairs are acquired for each operating condition. Cross-correlation processing is used to get the ensemble averaged velocity vector maps for particle flow.

The streamlines of the two investigation regions are shown in the Fig. 8 and Fig. 9. Because of the method for processing the experimental dates, the boundaries of the wall are not smooth. We drew the exact boundaries by handwork.

From Fig. 8 we can see that there is a large area of recirculation flow near the tongue at the low flow rate operating conditions. It is also can be seen that the change of the streamlines is negligible when the flow rate increases.

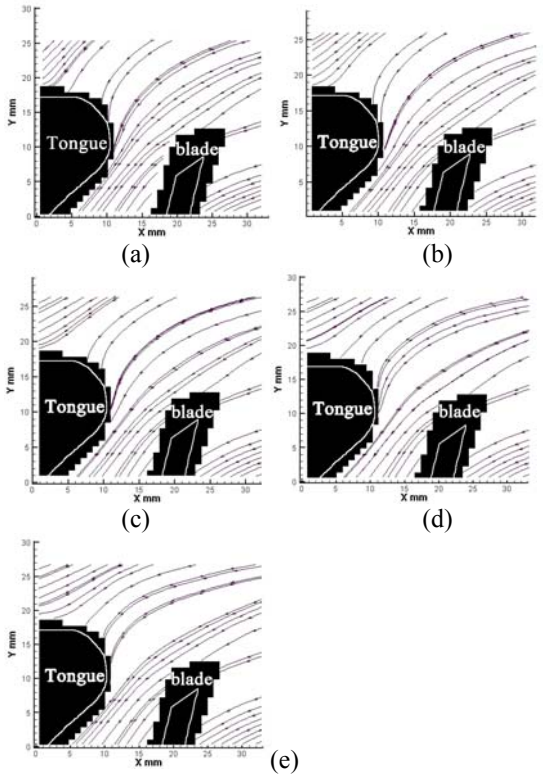

Fig. 8 Streamlines of absolute velocity for various operating conditions at tongue region (a)4L/m,(b)6L/m,(c)8L/m,(d)10L/m,(e)12L/m.

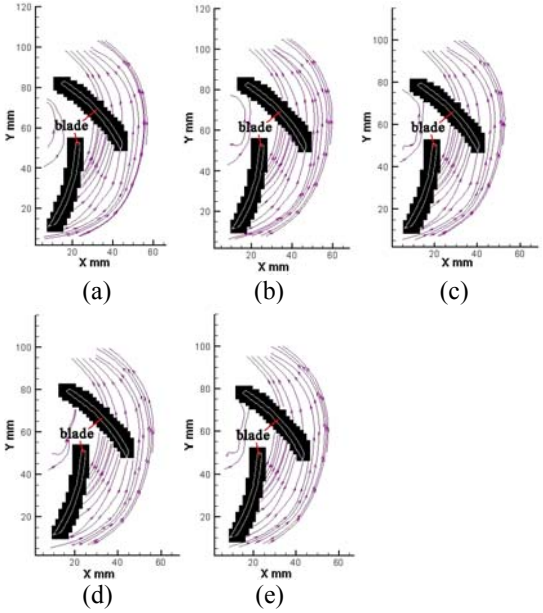

Fig. 9 Streamlines of absolute velocity for various operating conditions at impeller passage region (a)4L/m,(b)6L/m,(c)8L/m,(d)10L/m,(e)12L/m.

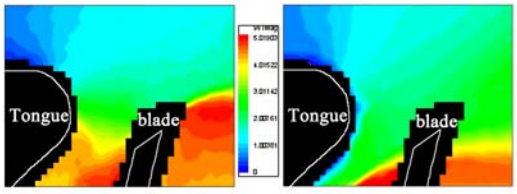

(a) 4L/min

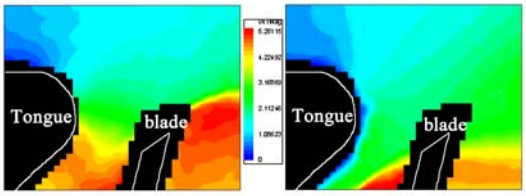

(b) 6L/min

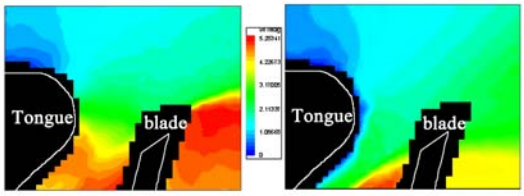

(c) 8L/min

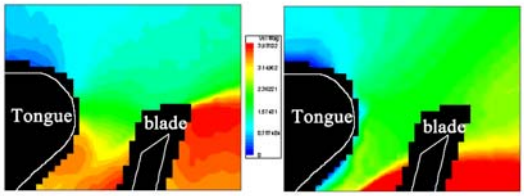

(d) 10L/min

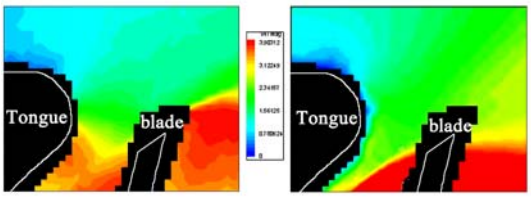

(e) 12L/min.

Fig. 10 Velocity magnitude distributions for various operating conditions at tongue region (Left by PIV measurement and Right by calculation)

The velocity magnitude distributions obtained by the PIV measurement and the calculation are shown in the Fig. 10 and Fig. 11. It is easily can be seen that the distributions acquired by measurement are similar with the ones acquired by calculation. Furthermore, the computational distributions are more homogeneous than the measurement results. So, we can conclude that the RNG k- ε turbulence model averages the velocity distributions and is not very suitable for capturing the flow detail information at low flow rate operating conditions, although it is in a very good agreement with the experimental results for the hydrodynamics

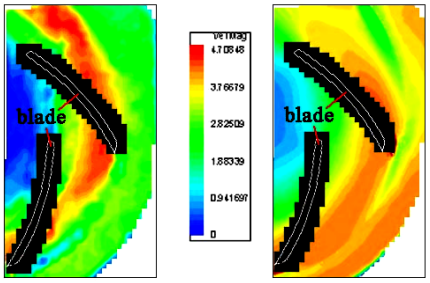

(a) 4L/m

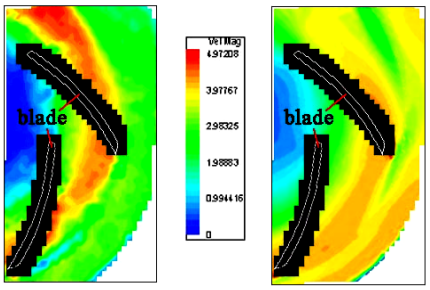

(b) 6L/m

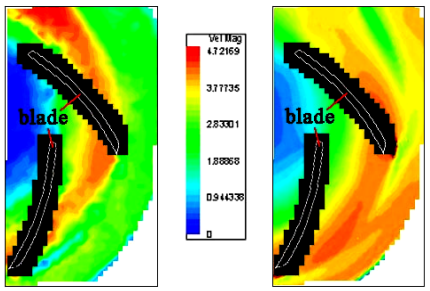

(c) 8L/m

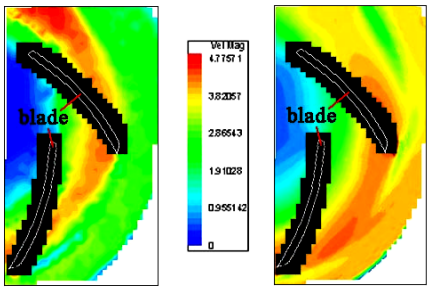

(d) 10L/m

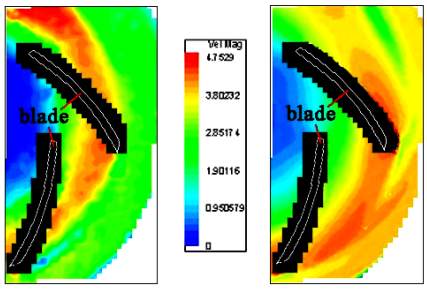

(e)12L/m

Fig. 11 Velocity magnitude distributions for various operating conditions at impeller passage region (Left-PIV measurement and Right- calculation)

performance prediction. Selecting the Large Eddy Simulations (LES) as the numerical method may get a better result. Meanwhile, we also can see that the velocity magnitude distribution in one passage is different to another as shown in Fig.11. This phenomenon is likely to be caused by the affection of the pump discharge location.

Conclusion

1) At the low flow rate operating conditions, the computationally predicted water head using the k-ε turbulence model is in a very good agreement with experimentally measured water head.
2) At the low flow rate operating conditions, the RNG k-ε turbulence model averages the velocity distributions and is not very suitable for capturing the flow detail information.
3) PIV measurements show that the flow status in one passage is different to another.
4) There is a large area of recirculation flow near the tongue at low flow rate operating conditions

Acknowledgments

This work has been supported by the National Natural Science Foundation of China (No.50676044), the China Postdoctoral Science Foundation (2006035267) and the Tsinghua Thermal Engineering Department Foundation.

References

1) Burgreen GW, Antaki JF.: CFD-based design optimization of a three-dimensional rotary blood pump. American Institute of Aeronautics and Astronautics (AIAA) Paper 96-4185, Proc 6th Symp on Multidisciplinary Analysis and Optimization, Bellevue, WA, pp. 1773-1778, 1996.
2) Burgreen GW, Antaki JF, Butler KC.: CFD-based design optimization of the outlet stator of a rotodynamic cardiac assist device. American Institute of Aeronautics and Astronautics (AIAA) Paper 98-4808, Proc 7th Symp on Multidisciplinary Analysis and Optimization, St Louis, MO, pp. 818-824, 1998.
3) Li Jinwei, Liu Shuhong, Luo Xianwu, Wu Yulin.: Viscous flow field in a mini pump. *J Tsinghua Univ. (Sci&Tech)*, Vol 47, No.5, pp. 682-685, 2007.
4) Nicholas Pedersen et al.: Flow in a Centrifugal Pump Impeller at Design and off-design conditions—Part I: Particle Image Velocimetry (PIV) and Laser Doppler Velocimetry (LDV) Measurements. *Journal of Fluids Eng.* Vol. 125, pp. 61-72, 2003.
5) J. R. Kadambi et al. : Investigations of Particle Velocities in a Slurry Pump Using PIV: Part 1, The Tongue and Adjacent Channel Flow. *Journal of Energy Resources Technology*. Vol. 126, 2004, pp. 271-278
6) Adrian, R. J.: Particle Imaging Techniques for Fluid Mechanics, *Annu.Rev. Fluid Mech*. 23, 1991, pp. 261–304
7) Keane, R. D., and Adrian, R. J.: Theory of Cross-Correlation Analysis of PIV Images, *Appl. Sci. Res.* 49, 1992, pp. 191–215.